Monte Carlo Modeling of Amorphous Polymer Deformation: Evolution of Stress with Strain

Clarence Chui† and Mary C. Boyce*

Department of Mechanical Engineering, Massachusetts Institute of Technology, Cambridge, Massachusetts 02139

Received September 29, 1998; Revised Manuscript Received March 16, 1999

ABSTRACT: A three-dimensional polybead model of the structure and large strain deformation of amorphous polymeric networks is constructed and evolved via Monte Carlo techniques. The model has successfully simulated various deformation conditions and been found to qualitatively capture the proper state of deformation, rate of deformation, and temperature dependence of real amorphous polymeric materials. Partitioning of the stress calculations indicates that strain softening following yield is a result of the evolution of intermolecular contributions to the response whereas the strain hardening phenomenon is a result of evolution in the intramolecular contributions. These calculations provide a fundamental basis for development of continuum-level plasticity models and, indeed, support assumptions currently used in successful constitutive models of the elastic−viscoplastic behavior of polymers.

1. Introduction

The underlying mechanisms of inelastic deformation in amorphous polymers remain an open question. The difficulties plaguing the task of probing the basic mechanisms governing amorphous polymer behavior stem from the complexities of the microstructure that dominates the response of the material. The typical structure for an amorphous polymer is that of an entangled network of long linear chains. The entangled network is rather random in nature in that the manner in which the atomic constituents of the chains are packed together resembles that of an atomic glass or "frozen" liquid. In contrast to atomic glasses, additional complexities are introduced by the connectivity of the polymer chains which constrain the motions of the atoms. Given that intrachain interactions are known to be at least 1 order stronger than interchain interactions,[1,2] mechanisms that govern the mechanical response of amorphous polymers as manifested in the stress−strain behavior must be consistent with the kinematic constraints of the chain structure. These topological complexities make direct experimental identification of these mechanisms extremely difficult. Understanding the contribution of the inter- and intramolecular interactions to the mechanical stress−strain behavior can provide a better basis for continuum-level modeling, as well as provide a more fundamental understanding of the connection between structure and properties in polymers.

The stress−strain behavior of amorphous polymers is observed to depend on strain rate, temperature, pressure, and state of strain (see Crist[3] and Boyce and Haward[4] for recent reviews). As shown in the experimental uniaxial compression data of Figure 1, the true stress−true strain behavior is characterized by an initial linear elastic response, followed by a nonlinear elastic transition to yield, followed by yield, followed by strain softening (a drop in the yield stress with plastic strain), and followed by strain hardening (an increase in the yield stress with plastic strain). The yield stress is found to increase with increasing strain rate, decreasing temperature, and increasing pressure. The post yield strain hardening behavior is found to strongly depend on the state of deformation (Arruda and Boyce[5]). The state of deformation dependence is also shown in Figure 1, where both uniaxial and plane strain compression true stress−true strain behavior is depicted.

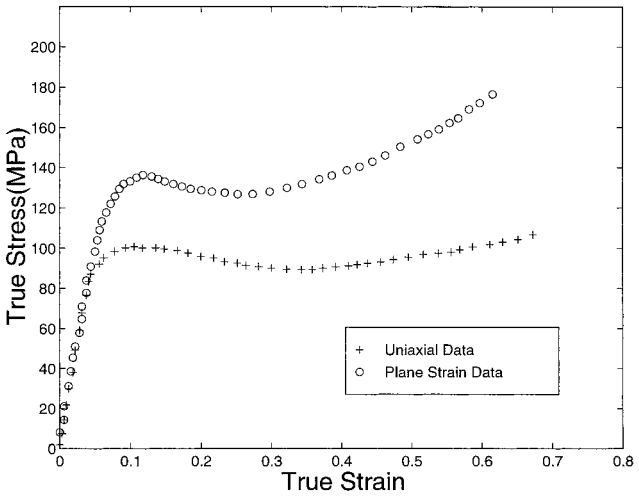

Figure 1. State of deformation dependence of mechanical response for PMMA. Responses under uniaxial compression and plane strain compression conditions are shown.

Any successful model for the inelastic deformation of amorphous polymers, whether it be on a continuum level or a molecular level, must be able to capture the dependence of the stress−strain behavior on rate, temperature, pressure, and state of deformation. In this paper, a new approach to modeling the structure and deformation of amorphous polymers on a molecular level is presented utilizing Monte Carlo (MC) techniques. The proposed model will be shown to capture the significant dependencies of the stress−strain behavior and thus provide a window into the underlying mechanisms. Below, relevant background on various modeling approaches is first reviewed; the modeling approach used in this work is then detailed. Results from the model

† Now at Exponent, Inc., Natick, MA.

10.1021/ma9815399 CCC: $18.00
Published on Web 05/13/1999

including the dependence of the stress−strain behavior on rate, temperature, and state of deformation are then presented; the relative contributions of inter- and intramolecular interactions to the macroscopic stress−strain behavior as well as the relevance of these results to continuum-level constitutive models are discussed.

2. Models of Amorphous Polymer Deformation

Many studies have been performed in attempts to understand the underlying physics governing the thermomechanical behavior of amorphous polymers.

Models of glassy state deformation have predominantly focused on the behavior of atomic/metallic glasses. Molecular dynamics (MD) simulations by Deng et al.[6] on atomic glasses find that plastic deformation occurs as a result of local rearrangements which produce shear transformations. They further find that the transformations essentially act as nucleation sites for additional transformations, the percolation of which eventually produces localized flow structure. Maeda and Takeuchi[7] and Srolovitz et al.[8] use molecular statics (MS) to model the deformation behavior of three-dimensional metallic glasses and employ the concept of atomic-level stresses in their analysis. They generally observe that plastic deformation is a result of highly localized heterogeneous atomic rearrangements which generate local stresses often considerably exceeding the applied stress.

Although the studies of atomic/metallic glasses provide interesting insights into the deformation behavior of relatively simple systems, the presence of chain connectivity makes the investigation of glassy polymer deformation considerably more difficult. The numerical investigations of Theodorou and Suter[9,10] using MS techniques represent the first attempts to model the mechanical response of glassy polymers. Although their studies are limited to probing the elastic properties of an idealized glassy polypropylene, the methods introduced by their efforts are used in several subsequent investigations including those of Mott et al.[11,12] and Hutnik et al.[13,14] Mott studies the plastic deformation of glassy polypropylene by using MS to probe the athermal shear response of packed single-chain systems. Mott's findings suggest that plastic deformation is a result of abrupt shear transformations which involve the cooperative motion of many degrees of freedom. Mott indicates that these cooperative motions are a consequence of the highly constrained nature of the amorphous chain structure. Hutnik's study of glassy polycarbonate produces similar results and indicates that cooperative motion is a feature of deformation accommodation in glassy polymers independent of the chemical specificity of the chain.

Simulations of glassy polyethylene are performed by Brown and Clarke[15] and McKechnie and Clarke[16] using MD techniques. The application of MD to the amorphous polymer deformation problem by these workers allows them to investigate the effects of thermal motion and attempt to correlate the obtained responses to experimental results. Although the deformation rates studied are much higher than those obtainable in experiments, the qualitative rate dependence and temperature dependence of the behavior under uniaxial tension conditions is in fairly good agreement with real amorphous polymer behavior. McKechnie's investigation probes the effects of initial chain configuration properties on the resulting mechanical response. The results suggest that both an increase in persistence length and fraction of trans conformers can independently contribute to enhanced strain hardening.

3. Modeling Methodology

Polymer structure and deformation can be modeled using several different approaches, principally including molecular statics, molecular dynamics, and Monte Carlo techniques. The level of detail incorporated in these modeling strategies varies from descriptions of electronic degrees of freedom to simple bead-spring representations of polymer chains. Several of these approaches are discussed extensively in Binder and Heerman.[17] Although the details of the various models are quite different, most require attention to four features: (1) specification of local interactions, (2) generation of network structure, (3) equilibration of the system to obtain a desired initial state, and (4) application of prescribed macroscopic deformation conditions.

The following sections describe the techniques employed in the present investigation to simulate amorphous polymer behavior. This work develops a Monte Carlo model which will simulate structure and deformation of a model amorphous polymer over a fairly wide temperature range by integrating techniques and individual model arguments used by others into a unified model.

3.1. Polybead Approximation and Local Interactions. Approaches in the form of a polybead approximation have been implemented for quite some time in models developed to probe polymer structure as well as mechanical behavior. The polybead representation assumes that the behavior of polymers is dominated by the fact that the material is composed of long chains with relatively rigid links. The chemical structure is represented by interacting beads located along the backbone of the chains. Examples of this approach include the studies by Curro[18] and Gao and Weiner[19,20] which consider the interactions of polybead chains at melt temperatures. The structural representation used in the present work is similar to that taken by Brown and Clarke[15] and Weiner and Gao[19,20] in that chemical structure is represented by polybead chains with bonded interactions specified so that physically realistic configurations can be achieved by the model.

In the polybead model, beads are connected by springs with bond lengths governed by a harmonic potential,

$$E_{\text{bond}} = \frac{1}{2}C_{ij}(r_{ij} - b)^2 \tag{1}$$

where r_{ij} is the distance between adjacent beads i and j, b is the equilibrium link length, and C_{ij} is the bond-potential coefficient.

The bond angle between any two adjacent links is determined by another harmonic potential of the form

$$E_{\text{ang}} = \frac{1}{2}\, C_{ijk}(\theta_{ijk} - \theta_{\text{o}})^2 \tag{2}$$

where θ_{ijk} is the bond angle between consecutive beads i, j, and k, θ_{o} is the equilibrium angle of the potential and C_{ijk} is the bond-angle-potential coefficient.

The torsion angle between the planes defined by consecutive beads i, j, k, and j, k, l which physically describes the rotation along the chain segment backbone is governed by a 3-fold cosine potential:

$$E_{\text{rot}} = \frac{1}{2} C_{ijkl}[(\cos 3\theta_{ijkl}) + 1] \tag{3}$$

where θ_{ijkl} is the backbone angle of rotation; and C_{ijkl} is the rotational angle potential coefficient.

The intermolecular interactions are described by a Lennard-Jones-type potential:[21]

$$E_{\text{int}} \begin{cases} = 4\gamma \left[\left(\frac{\sigma}{r_{ij}}\right)^{12} - \left(\frac{\sigma}{r_{ij}}\right)^{6}\right] \text{for } r_{ij} \le 1.4\sigma \\ = 0 \text{ for } r_{ij} > 1.4\,\sigma \end{cases} \quad \text{for } r_{ij} \le 1.4\sigma \tag{4}$$

where γ is the characteristic energy well of the potential, σ is the excluded volume radius, and r_{ij} is the distance between particles i and j.

The Lennard-Jones (LJ) potential facilitates the maintenance of a minimum particle spacing while providing the system with a source of long-range cohesion through its weakly attractive tail portion. A relatively short truncation distance is used for computational convenience, which still allows the qualitative effects of excluded volume to be represented. Also, first- and second-bonded neighbors along the backbone of the same chain are not affected by the intermolecular interactions whereas particles associated with other chains are always affected. Finally, it should be understood that the links and beads in the network are not meant to explicitly represent actual bonds present in polymer chains but are instead viewed as larger scale entities possibly representing groups of bonds or other aggregate molecular structures.

The forms and parameters associated with these interactions are chosen to be in accord with relationships established in previous models of molecular-scale behavior.[15,22] Namely, the bond lengths and angles are assumed to be nearly fixed whereas the backbone rotation is assumed to be relatively free. Table 1 shows the parameter values used for the interactions described in this section. The values are typical in that the relative scaling of bond stretching, valence angle bending, bond torsion, and intermolecular energies and dimensions are consistent with those adopted by Sylvester,[22] Brown and Clarke,[15] and Ogura and Yamamoto.[23]

3.2. Network Generation. The technique used to generate the polymeric network is a variant of the method established by Theodorou and Suter.[9] The chain contour is generated via a random walk process in which each bond in the chain is considered to be one step in the walk. The selected magnitude and direction of the bond vector is governed by the local interactions assigned to the system. As it is desirable to generate a system which is initially as close to equilibrium as possible, the bond vector lengths and bond angles used during chain growth are the equilibrium values specified by eqs 1 and 2, respectively. The dihedral angle is randomly selected to produce an initially unbiased distribution of conformers. The presence of intermolecular or excluded volume interactions are not considered during the chain generation procedure. Attempts to directly incorporate the effects of these interactions on the selected bond vector directions can lead to considerable difficulties.[24]

The network is constructed by considering an assembly of chains generated in the manner described above, with the origin of each chain being specified by the location of a generation "seed" which is placed within the simulation cell. By specifying the spacing of these seeds, networks of varying particle number density can be created. One simple way to ensure a relatively uniform distribution of chains and particles is to distribute the seeds within the cell in a cubic pattern as done in this work. Chains emanate from each seed via the random walk process until reaching a desired number of bonds. The locations of the seeds can be perturbed from the lattice sites to introduce additional randomness into the system. However, the random walk nature of the chain growth process has been found to provide an adequate degree of disorder for the system without the perturbation of seed coordinates.

Table 1. List of Typical Parameter Values

parameter	value
C_{ii}	1674 kJ/Å^2/mol
C_{ijk}	300 kJ/rad^2/mol
C_{ijkl}	11.7 kJ/mol
b	1.47 Å
θ_o	1.26 rad
σ	3.53 Å
γ	0.352 kJ/mol

To minimize size effects, periodic boundary conditions are prescribed for all cell directions. Although some artifacts are introduced into the simulation as a result of the periodicity condition in that cooperative motions of the chains/particles necessarily imply simultaneous cooperative motions of neighboring images, for processes which are rather localized in nature (i.e., involve only tens of particles), the interaction effects of images are negligible.

To form a well-connected network, the ends of the chain segments are attached to the nearest generation seed that is within a specified tolerance distance. By varying the size of the tolerance radius, the probability that a generation seed falls within the tolerance sphere, and thus the probability of a cross-linking occurrence, can be adjusted. A similar cross-linking occurrence criteria is implemented by Grest et al.[25] and Duering et al.[26] in simulations of end cross-linked polymer melts. Varying the number of chain segments generated, the maximum number of cross-links allowed at each seed, the number of links per segment, and the tolerance radius produces networks with a wide range of topological properties. The networks investigated in this study are limited to either single-chain systems or monodisperse networks allowing a maximum of four chains per generation seed (i.e., tetrafunctional cross-links) with segment loops not being allowed to form (i.e., a chain segment can not begin and end at the same bead), although this feature can very easily be included.

3.3. Evolution of Structure. Molecular statics, molecular dynamics, and Monte Carlo methods are the primary techniques used to evolve material models that account for the discrete nature of the material structure. MS methods attempt to find the configuration sampled by the model degrees of freedom through minimization of the system total potential energy. The minimum energy configurations found usually correspond to local minima near the initial configuration. Application of this technique to amorphous polymer simulations include the studies of Theodorou and Suter,[9,10] Mott et al.,[11] and Hutnik et al.[13] MD methods attempt to sample configuration and momentum phase space through the use of Newton's equations of motion. MD applications to amorphous polymer behavior include the deformation simulations of Brown and Clarke[15] and Gao and Weiner[19,20] and the structural simulations of Sylvester.[22]

In recent years, MC methods have become increasingly prominent in materials simulation studies. Generally, the techniques rely on the applicability of the view of material evolution as being stochastic in nature. MC algorithms draw heavily from probability theory and attempt to sample the most probable portions of the system's configuration phase space. As most of these methods are based on sampling from statistical mechanical ensembles, temperature is explicitly incorporated and allows the technique to account for thermal motion. Applications of MC to polymers include the investigations of Curro[18] and Lobe et al.[27] As discussed below, variations on the MC technique introduced by Metropolis et al.[28] are used in the present study to probe the deformation behavior of amorphous polymers.

3.3.1. Metropolis Algorithm. The current work adapts the basic Monte Carlo technique introduced by Metropolis[28] in which the potential energy of the system is calculated from the initial configuration of the structure (generated by the network algorithm). Evolution of the structure or particle motion is introduced by selecting a particle and perturbing its position by a small random displacement. The energy of the structure is then recalculated, and the perturbed configuration is accepted as the new configuration with a probability of

$$p = \min\left\{1, \exp\left[-\frac{(E_{i+1} - E_i)}{kT}\right]\right\} \tag{5}$$

where E_i is the potential energy of the current configuration, E_{i+1} is the potential energy of the perturbed configuration, T is the absolute temperature, and k is Boltzmann's constant.

In theory, by running the algorithm for a sufficient number of cycles (where a cycle is defined here as perturbing each particle once), the system continues to evolve and eventually reaches a statistical steady-state consistent with the constant particle-number/volume/temperature ensemble (NVT). Variations on the algorithm can be introduced to allow sampling of other ensembles (e.g., NPT, NVE, etc.) (see Heerman[29]). Because the algorithm requires some number of cycles before reaching the equilibrium sampling condition, accumulation of property data is typically not performed until most of the important thermodynamic quantities (i.e., energy, pressure, etc.) appear to reach a statistical steady-state condition. Exactly when the steady-state is reached is often difficult to determine, particularly at low temperatures when the algorithm converges quite slowly.

In practice, the magnitude of the perturbation displacement is often adjusted to make the algorithm efficient. This is done because very large displacement magnitudes generally produce low acceptance rates whereas very small displacement magnitudes produce high acceptance rates but tend to make the system sample phase space very slowly. For the present calculations, the displacement magnitude is adjusted so that the percentage of accepted moves remains between 45 and 55%.

Given that the deformation of amorphous polymers at low temperatures is inherently a nonequilibrium process, the Metropolis algorithm, as applied in the present calculations, requires reinterpretation. The simulations presented consider the algorithm as a minimization procedure in which the lowest energy configuration attainable is governed by the amount of available thermal energy and the number of Monte Carlo cycles considered. For simulations of structures being rapidly quenched from the melt to the glassy state, the rapid cooling process effectively traps the amorphous structure in a metastable state by making the algorithm converge to a local energy minimum in configuration space. In theory, the system eventually "breaks out" of the local minimum and continues towards the global minimum over a large enough number of cycles. However, the simulations are typically stopped once a local minimum is reached so that the mechanical behavior of the nonequilibrium or "frozen" liquid like behavior of the polymer structure can be sampled in subsequent deformation simulations.

3.3.2. Preparation of Initial Structure. The initially generated structures are not in equilibrium and must be relaxed before deformation is applied. Annealing and quenching are critical in that they strongly affect the initial state of the network and thereby determine the subsequent properties of the system. This is especially true at low temperatures for which the Metropolis algorithm samples very limited regions of phase space. The annealing and quenching procedure followed in this work can be summarized in 7 steps:

1. The Metropolis algorithm is applied at high temperatures ($T^* \approx 50$ where $T^* = kT/\gamma$) in the NVT ensemble before the introduction of any intermolecular interactions to allow the bonded interactions to reach a statistical equilibrium.

2. Intermolecular interactions are introduced through the use of a modified soft sphere potential with the radius being gradually increased while still running in the NVT ensemble.

3. The Lennard-Jones potential is introduced, and the system is allowed to continue equilibrating in the NVT ensemble at high temperatures.

4. The system is compressed to the approximate target density through an alternating sequence of affine volumetric contraction jumps followed by some number of minimization cycles at high temperatures.

5. The temperature is then reduced to the desired value, and the system continues to relax at that temperature in the NVT ensemble.

6. The system is then relaxed in the NPT ensemble under compressive pressures to remove excess volume.

7. The pressure is then removed, and the system is allowed to relax under pressure-free conditions in the NPT ensemble until approximately reaching a steady state in the energy and volume behavior.

Finally, the systems are loaded and unloaded under uniaxial compression conditions up to a true strain of -0.1. This deformation preconditioning has the effect of removing any remaining excess volume and serves to eliminate artificial structural instabilities. The magnitude of the preconditioning strain was empirically found to be large enough to create stable systems while still small enough so that orientation-related anisotropy was not induced in the network. This procedure appears to be rather effective in creating systems which behave like typical polymers in the sense that most thermomechanical phenomena are qualitatively reproduced.

3.4. Application of Macroscopic Deformation. Deformation is applied to the model via a series of strain increments followed by a number of Metropolis minimization cycles. Incremental affine motion is used as an initial guess for the particle positions during the strain increment with the subsequent minimization

cycles allowing the particles to find energetically favorable positions (as dictated by the constraints of the local chain environment), thus producing a deformation field which is inhomogeneous. The minimized configuration is then used as the reference configuration for the next strain increment. The number of minimization cycles specified are such that deformation is continually applied before the system is allowed to fully thermodynamically equilibrate. Varying the number of minimization cycles between increments allows the model to qualitatively probe the effects of deformation rate changes.

Magnitudes of strain increments explored range from true strains of 0.001 25−0.01. Strain increments near 0.01 are found to be too large to give realistic responses, with energy changes observed during these simulations indicating that intermolecular energy values become so large that the subsequent configurations sampled by the particles may be physically unrealistic. Strain increments of 0.0025 or less are found to produce better behaved energy measures. Trials comparing systems using 0.001 25 increments and 0.0025 are found to exhibit little difference in their behavior when the number of minimization cycles between strain increments are specified so that the total number of cycles attempted during each simulation is the same. The results presented in this investigation are obtained from systems employing the 0.0025 strain increments with typical minimization schedules specifying 50−100 cycles per strain increment. Techniques employing simple shifting of displacement-controlled boundaries were also explored but found to require a significant number of minimization cycles ($\gg$100) between shifts before artificially dense or sparse regions (i.e., density "shocks") generated by the boundary motion diffused through the system. The appearance of physically unrealistic density shocks are observed by Ogura and Yamamoto[23] using simple boundary shifting and molecular dynamics methods to simulate polymer deformation at extremely high strain rates.

Simulation of various states of deformation (e.g., uniaxial compression, plane strain compression, uniaxial tension), requires different combinations of traction and displacement-controlled boundaries. Calculation of internal stresses is facilitated through the use of the virial stress theorem from statistical mechanics[21] which computes stresses by calculating all of the lines of force which cross a plane "cut" in the network and averaging this over all possible cuts. The inclusion of thermal motion effects leads to the following form:

$$\tau_{ij} = \frac{1}{V}\left[- NkT\delta_{ij} + \sum_m \left(\frac{1}{r_m}\right)\left(\frac{\partial}{\partial r_m} E(r_m)\right) x_i(m)x_j(m)\right] \tag{6}$$

where τ_{ij} is the ij component of stress, V is the system volume, N is the number of particles in the system, k is Boltzmann's constant, δ_{ij} is the Kroneker δ, r_m is the distance between the mth interacting particle pair, E is the potential energy due to the mth pair interaction, x_i and x_j are the ith and jth components of the vector separating the mth pair of particles.

The cell dimensions are adjusted every few MC minimization cycles to maintain consistency between the internal stress state (calculated via the virial stress theorem) and the desired combination of externally applied boundary tractions and displacements. These adjustments are facilitated through the use of a closed-loop feedback procedure which interpolates between the dimensions of the current configuration and those of a "trial" configuration. The procedure is further simplified by neglecting the effects of shear deformations on the cell (i.e., the axes used to define the shape of the cell are constrained to remain orthogonal to one another), which from early trials were found to be negligible for the systems considered.

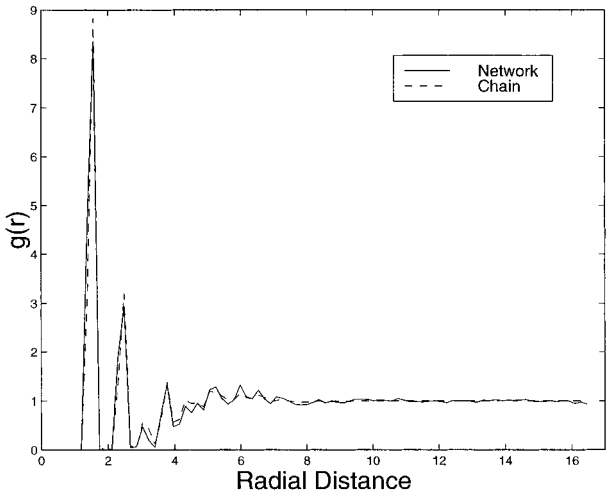

Figure 2. Comparison between pair radial distribution functions computed for a single chain and a network.

4. Simulation Results

Simulations involving a variety of network parameters were implemented to probe the sensitivity of the above-proposed methods to changes in network topology. Both single-chain systems and multiple-chain systems involving 1000−12 000 particles were simulated. Cross-linked networks typically consisted of 250 chains with 40−50 particles per chain. Cell dimensions for these networks ranged from 71 to 77 Å on a side with the specific values depending on the temperature of the system being simulated. The reduced densities (defined as $\rho^* = N\sigma^3/V$) under pressure-free conditions were approximately 1.4, 1.3, and 1.1 at reduced temperatures (defined $T^* = kT/\gamma$) of 0.284, 1.42 and 2.84, respectively.

4.1. Validation of Initial Structure. The networks display spatial correlations in structure appropriate for glassy materials with strong short-range correlations representative of inter- and intrachain first- and second-neighbors and weak long-range correlations representative of random motion. Figure 2 depicts pair radial distribution functions of a single chain and of a network system computed with the present model. The distributions illustrate the short-range order resulting from the relatively rigid bond lengths and angles and the weak spatial correlation among particles at large topological distances. The calculated pair radial distribution functions compare favorably with those found from MD simulations by Sylvester[22] on polypropylene, MS investigations by Hutnik[14] on polycarbonate, and experimental measurements by Wignall and Longmann[30] on polycarbonate and poly(ethylene terephthalate), indicating that the polybead approximation does not prohibit the model from reproducing basic structural features observed in simulations for which specific chemical structures are modeled.

Bond length and angle distributions indicate that on average the bonds are being stretched in tension and

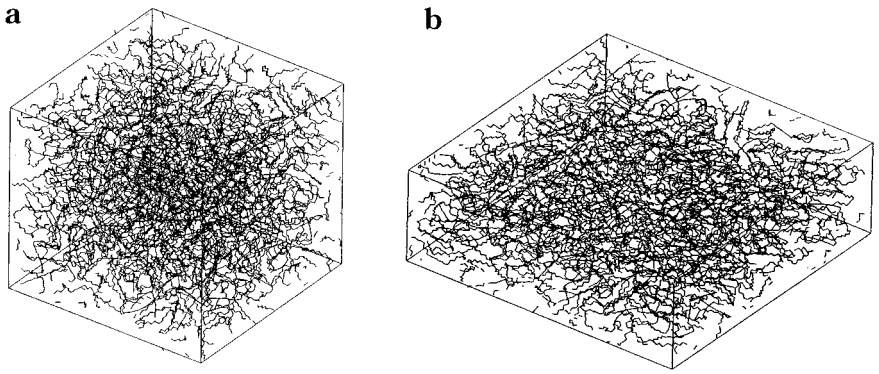

Figure 3. Plot of periodic cell and network bond vectors: (a) undeformed configuration and (b) after 70% true strain under uniaxial compression conditions.

that the bond angles are on average being flexed "open". This shifting of the distributions away from the equilibrium bond length and bond angle values is due to the local effects of intermolecular repulsive interaction. Torsion angles positioned in the closed (i.e., gauche) configuration induce repulsive steric interactions which tend to produce locally stretched bonds and flexed bond angles at all temperatures investigated. Similar results are found in the simulations by Sylvester on amorphous polypropylene above and below the glass-transition temperature. As in the pair radial distribution calculations, the consistency of the polybead results with chemically specific simulations suggests that the observed features of bond length stretching and bond angle flexing are general characteristics of entangled chain structures. Comparisons between bonded distributions of single chain and network systems show that the long-chain structures contain a small fraction of bond angles which are flexed to a greater extent than is attributable to thermal motion, indicating that the constraints produced by the self entanglement of the long chain locally hinder relaxation of a small number of bond angles. Simulations on polybead type chains probing relaxation behavior of multiple-chain systems at melt temperatures appear to suggest that reptation type processes occurring over long time scales would eventually eliminate the stretched and flexed bond and bond angle outliers observed in the single-chain simulations. However, the limitation of present computational resources to short time scales and the approximation of long-chain structures through the use of a single periodic chain makes a direct interpretation of the results in that context extremely difficult. In contrast to the single chain systems, the presence of free ends and relatively short chains in the cross-linked networks appears to provide the chains with enough mobility so that any extended bonds or flexed bond angles produced during preparation of the structure have sufficient time to relax out of the system during the annealing/equilibration steps.

4.2. Stress-Strain Behavior. By looking at the mechanical response of the system at low temperatures, the general nature of how the system deforms in the glassy state is probed. The results in Figures 3−5 are obtained from a constant strain rate uniaxial compression simulation of a system consisting of 250 chains with 48 particles/chain at a reduced temperature of $T^* = 0.2841$. The deformation increments in the simulation are applied in 0.0025 strain increments with 100 MC cycles allowed between each strain increment. Figure 3 displays the bond vectors of the network and boundaries of the periodic cell before and after 0.7 true strain is applied. The stress−strain response shown in Figure 4 has many of the important features observed in glassy polymers. The response is initially stiff and linear but eventually leads to nonlinear behavior near a strain of 0.02. The stress continues to increase in a nonlinear fashion until a plateau in the response is reached near a strain of 0.11. The peak is followed by an extended region between 0.15 and 0.5 strain where the stress decreases. In the strain range of 0.6−0.7 the response

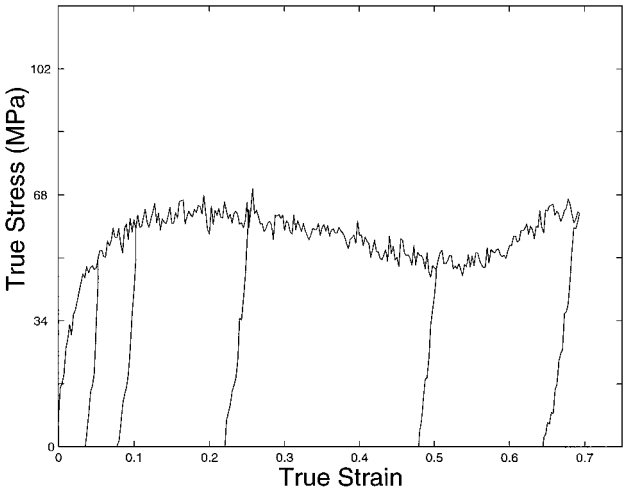

Figure 4. Simulated stress−strain response of large network under uniaxial compression. (Note that several unloading paths are shown).

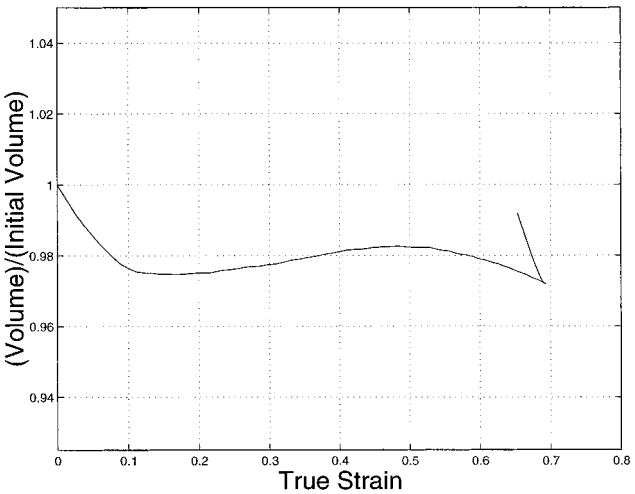

Figure 5. Volume−strain response of large network under uniaxial compression.

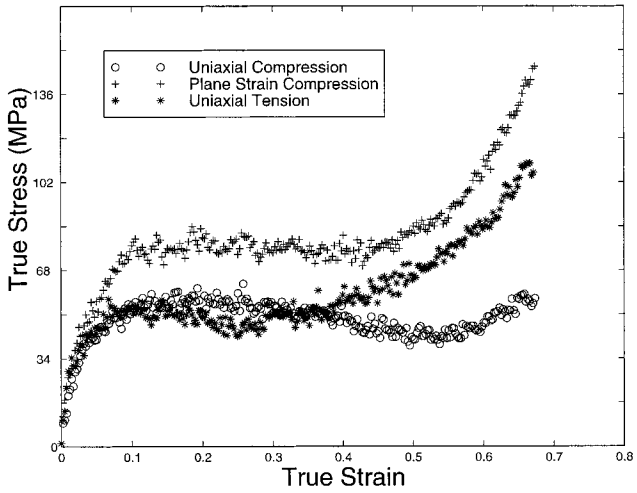

Figure 6. Macroscopic response of the network under uniaxial compression, plane strain compression, and uniaxial tension.

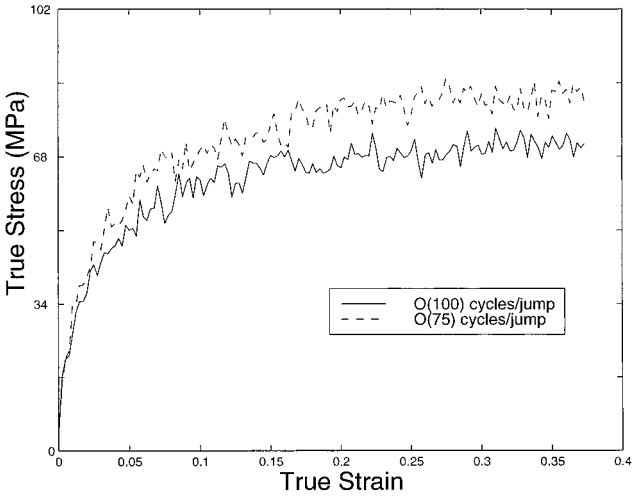

Figure 7. Rate dependence of large network during uniaxial compression. The rates are specified to obtain an approximately fixed number of Monte Carlo cycles during each relaxation step. Higher strain rates correspond to fewer numbers of cycles.

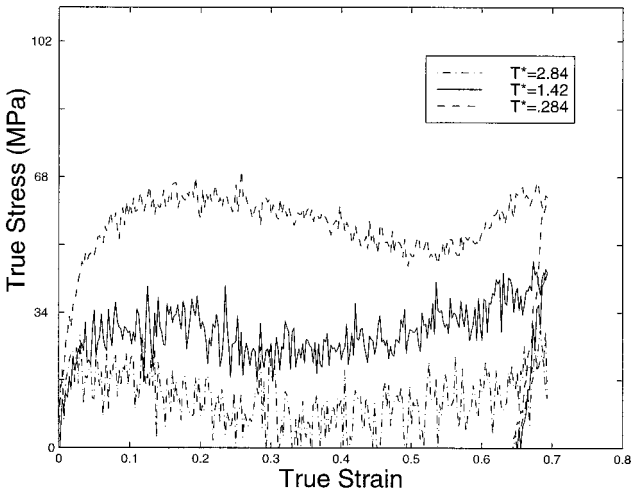

Figure 8. Temperature dependence of large network during uniaxial compression.

begins to stiffen as the system exhibits strain hardening behavior as indicated by the gradual increase in stress. The nonlinear unloading path leaves the system with an accumulated plastic strain of 0.65. Several other unloading paths are also shown in the figure to demonstrate that the model exhibits inelastic behavior and that the unloading behavior is noticeably nonlinear even after initial strain of less than 0.2. Although the exact strain at which the stress peak occurs in this example is higher than values observed for real polymers, the simple polybead representation qualitatively captures all of the salient features that define the characteristic behavior of these types of materials.

The model also approximately captures the well-known constant volume condition observed during plastic flow (Figure 5). Initially, the system accommodates applied deformation through the gradual compaction of the particles exhibiting a Poisson ratio of 0.39. After a strain of approximately 0.1, the material begins to flow in a volume-conserving manner as the competition between continual compaction of the particles and the energetic infeasibility for doing so balance one another; this coincides with the yield point and confirms the distortional nature of plastic deformation of polymers.

4.2.1. State of Deformation Dependence. Figure 6 depicts the behavior of the network under uniaxial tension, uniaxial compression, and plane strain compression conditions. The constraint stresses required to maintain the plane strain condition contributes to the elevated response of the system by forcing all deformation to be accommodated by the lone unconstrained direction. (Using a Mises equivalent yield stress measure, the equivalent yield stresses are found to be 56, 60, and 70 MPa in uniaxial tension, uniaxial compression, and plane strain compression, respectively. Note that the applied pressure in these cases are −19, +20, and +40 MPa respectively. These results clearly show that yield stress increases with pressure.) The results clearly show that the macroscopic flow stress is a function of mechanical constraint with the high pressures of plane strain deformation producing the highest equivalent yield stress and the negative pressures of uniaxial tension producing the lowest. At large strains (i.e., strain > 0.4), the anisotropic evolution of orientation in the network increases the differences among the three states of deformation. The simulation prediction of the difference between uniaxial and plane strain compression behavior compares well with that observed experimentally, as reported earlier in Figure 1. The predicted similarity in strain hardening under uniaxial tension and plane strain compression conditions is also in accord with experiments (for example, see Boyce et al.[31] and Arruda and Boyce[5]).

4.2.2. Rate of Deformation and Temperature Dependence. As discussed in the methodology section, the model is capable of qualitatively capturing rate of deformation effects on mechanical response. Figure 7 displays the response of the network uniaxially compressed at two different rates. Decreasing the number of MC cycles allowed between strain increments mimics deformation at higher rates. The data illustrate that higher applied deformation rates tend to elevate the yield/flow stresses obtained from the system. Temperature effects are also captured by the model as shown in Figure 8. The data show a general trend of flow stress decreasing with increasing temperature.

5.0. Contribution of Bonded and Nonbonded Interactions

5.1. Evolution of Internal Energy. The contribution of the various interactions to the stress−strain

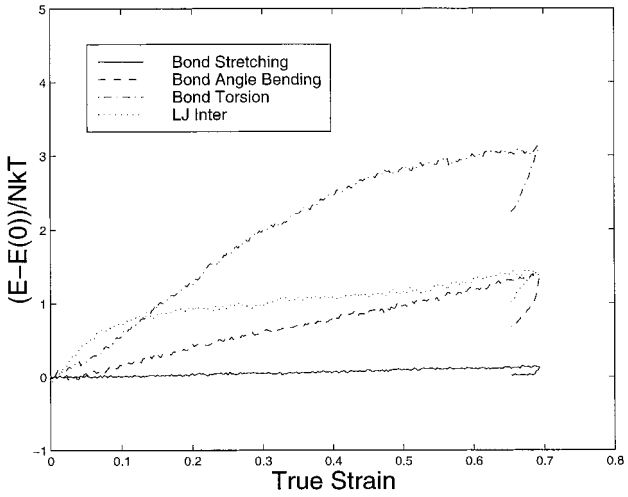

Figure 9. Evolution of normalized internal energy changes during uniaxial compression simulations of large network at $T^* = 0.2841$.

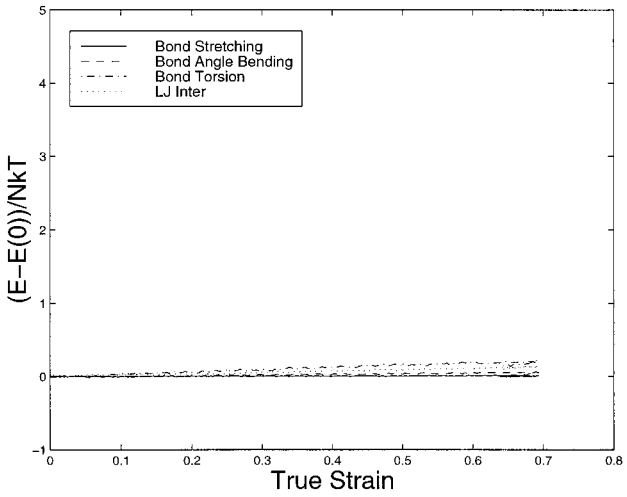

Figure 10. Evolution of normalized internal energy changes during uniaxial compression simulations of large network at $T^* = 2.84$.

behavior can be examined further by monitoring the evolution of internal energy. Figure 9 displays a normalized measure of internal energy changes occurring during loading and unloading at $T^* = 0.2841$. At small strains ($0 <$ strain < 0.03), the energy changes are dominated by the increase in intermolecular potential energy, a result consistent with the decrease in mean particle spacing induced during the elastic compaction stage of deformation. Beyond a strain of 0.03, the bonded energies begin to increase; the relative rate of increase reflects the relative compliance of the particular degree of freedom (i.e., torsion interactions undergo greater changes than the stiff bond stretching interactions). Near a strain of 0.1, where the stress peak occurs, the bond torsion energy increases rapidly and continues to do so until approaching a plateau near a strain of 0.6. This transition near a strain of 0.1 coincides with the leveling off of the intermolecular energy and the initiation of constant volume flow behavior, suggesting that the network is accommodating deformation through the activation of some kinematic mechanism involving bond rotations for which bond rotation is the most accessible degree of freedom. After unloading, the bond stretching energy returns to its initial value, reflecting the relatively stiff interaction specified for the stretching degree of freedom. However, the other energy quantities remain at higher than predeformation levels, indicating that mechanical work promotes the accumulation of internal energy which can presumably be released through annealing. The temperature effect on the evolution of internal energy storage is shown in Figure 10 which shows the normalized energy changes at $T^* = 2.841$. A comparison between the results displayed in Figures 9 and 10 shows that internal energy changes are much less pronounced at higher temperatures. The normalization by NkT accounts for the initial potential energy storage induced by thermal motion.

5.2. Partitioning of Stress. Macroscopic stress consists of contributions from thermal motion, bonded forces, and intermolecular forces. Calculations for single-chain and network systems under pressure-free conditions at various temperatures show that bonded contributions are always tensile and nonbonded contributions are always compressive (i.e., repulsive), suggesting that the "locking in" of tensile bonded forces and compressive intermolecular forces is a general feature of densely entangled chain systems. There appears to be some ambiguity regarding the issue of stress partitioning in previous studies. Although simulations like those performed by Mott et al.[11] and Hutnik et al.[13] help confirm that glassy systems possess a distribution of internal misfit stresses, relatively few studies have probed issues regarding the relative contributions of different types of interactions (i.e., bonded and nonbonded) to the total stress state of amorphous polymeric systems. Studies by Gao and Weiner[32] on freely jointed polybead chains in randomly oriented melts suggest that at high reduced densities, the bonded and nonbonded contributions to the total deviatoric (i.e., distortional) stresses are compressive and tensile, respectively, a result apparently at odds with the present observations. However, Gao and Weiner obtain their results at high densities using a constant volume ensemble which may generate large enough hydrostatic pressures that the total stress contributions from both bonded and nonbonded sources are negative. Whether this is in fact so is not clearly stated in their investigations. The study conducted by Theodorou and Suter[9] also attempts to address this point by calculating the bonded and nonbonded contributions to the total stress in amorphous polypropylene. Although the total stresses obtained by the initial structures are characterized by the presence of an initial nonzero stress "noise", Theodorou and Suter generally find that the bonded contributions to total stress are slightly compressive and the nonbonded contributions are slightly tensile. They further suggest that these results are a general feature of amorphous polymer structures and stand as strong evidence for the validity of Flory' assumption that polymer chains at high concentrations behave ideally. However, their use of initial densities fixed to correspond to values found experimentally at temperatures of interest indicates that the initial chain-packing arrangements obtained may not be appropriate for the model parameters selected when thermalized via alternative methods like MD or MC under pressure-free conditions. The MD study by Sylvester[22] on amorphous polypropylene using parameters similar to those of Theodorou and Suter demonstrates this point clearly by showing that under atmospheric pressure conditions the bonded contributions to the total stress are markedly tensile for temperatures ranging from below the glass transition to

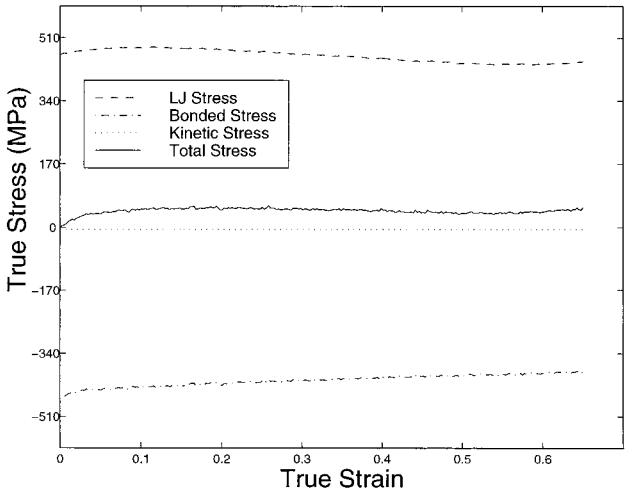

Figure 11. Partitioning of stress for network at $T^* = 0.2841$ under uniaxial compression conditions. (Note that compressive stress is being plotted so that the actual signs of the stresses are the opposite of what is shown in the figure)

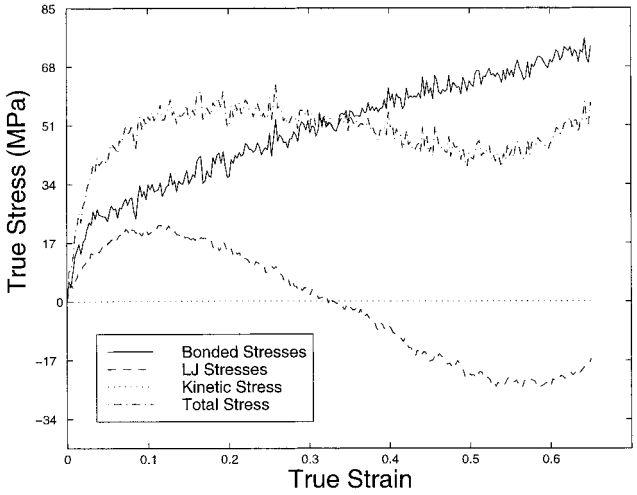

Figure 12. Partitioning of stress for network at $T^* = 0.2841$ under uniaxial compression conditions with data shifted for clarity.

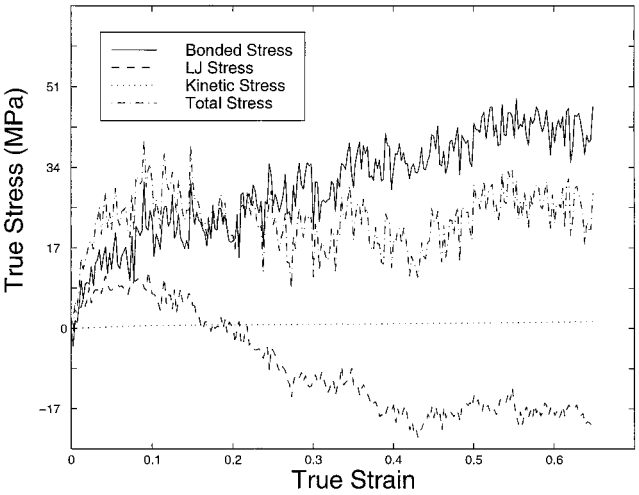

Figure 13. Partitioning of stress for network at $T^* = 1.42$ under uniaxial compression conditions with data shifted for clarity.

temperatures well above it. That this feature in the Sylvester results and in the present results is not simply an artifact of the strong steric hindrances induced by the selected model parameters is shown from simulations of systems at two temperatures under pressure-free conditions using an $L^* = \sigma/b$ value of 1.75 instead of the value of 2.4 utilized in other systems. $L^* = 1.75$ corresponds to a system in which the bias towards the trans state due to intermolecular interactions is nearly negligible. Although the magnitudes are greatly reduced by the change in L^*, the signs of the stresses follow the same patterns as those found for the biased cases, suggesting that the locking in of tensile bonded forces and compressive intermolecular forces is a general feature of densely entangled chain systems.

Figure 11 displays the individual contributions to stress (i.e., thermal, bonded, intermolecular) for a network deformed under uniaxial compression conditions at $T^* = 0.2841$. The figure shows that the initial absolute values of the bonded and nonbonded components are much larger than the maximum stresses obtained from the overall response. By shifting the individual components so that the initial values for each contributor are 0, the evolution of each stress can be more clearly viewed (Figure 12). Figure 12 shows that the initially stiff elastic response ($0.0 <$ strain < 0.07) has two significant contributions from both inter- (LJ stress) and intramolecular (bonded stresses). The departure from this initially stiff response signals the onset of plastic flow (yield) and is characterized by a rollover and plateauing of the intermolecular contributors to stress followed by a gradual decrease with increasing strain. Upon yield, the bonded contribution continues to increase but at a slope much lower than that of the initial stiff elastic regime; during plastic deformation, this monotonic increase in stress from the bonded interactions is a result of the rotation of the bond vectors toward the principal stretch directions. These results demonstrate that the material strain softening observed in numerous experimental studies is a result of a decrease in the intermolecular barrier to deformation, as will be examined further in the Discussion. At $T^* = 1.42$ (Figure 13), the pattern is similar in that the intermolecular component of stress is the sole contributor to the strain softening response, the intramolecular component increases monotonically, and both components contribute significantly to the total stress in the small strain (strain < 0.1) regime. The pattern continues at $T^* = 2.841$, as shown Figure 14 with the exception that at this temperature the intermolecular component of stress monotonically decays to a steady state (i.e., there is no initial increase in the intermolecular component before it begins to soften).

6.0. Discussion

6.1. Macroscopic Stress−Strain Behavior and Internal Energy Evolution. Physical interpretation of the macroscopic behavior obtained from the simulations requires an understanding of the material state/structure represented by the model at various temperatures and strain rates. At low temperatures or sufficiently short time scales, the behavior is governed by the inherent resistances of the material structure. In this regime, the structural barriers to deformation/flow do not evolve appreciably over the time scale of interest. It is in this regime that the description of deformation as a stress-biased, thermally activated process is most applicable.[33,34] This "isostructure" response is characterized by the essentially fixed nature of deformation energy barriers where direct use of absolute rate theory to describe flow is justified.

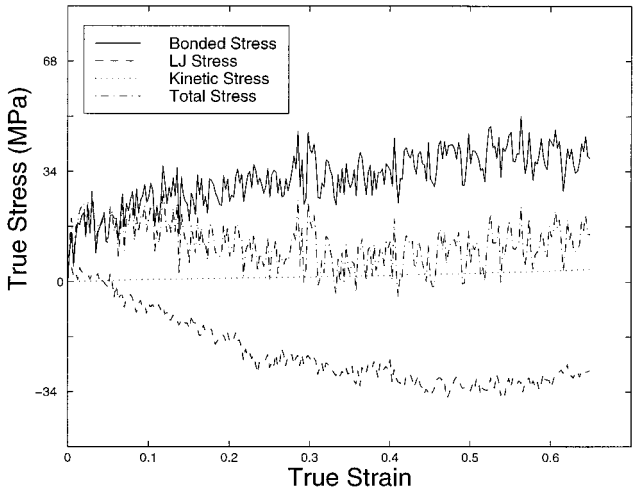

Figure 14. Partitioning of stress for network at $T^* = 2.84$ under uniaxial compression conditions with data shifted for clarity.

At the other extreme, deformation conditions involving very high temperatures or sufficiently long time scales are characterized by structural relaxation phenomena that allow the material to readily reach thermodynamic equilibrium. Behavior in this regime is not adequately described by the conventional thermal activation framework because energy barriers formed by the structure may be rapidly modified because of relaxation phenomena. Physical theories[35] explicitly consider the relaxation of the structure in obtaining a model of polymer networks at high temperatures. Statistical theories of rubbery networks assume that the behavior is adequately described by equilibrium thermodynamic arguments where entropic forces are the dominant contributor to the mechanical behavior.

Behavior in the transition region is characterized neither by isostructure behavior or rapid structural relaxation. Instead, the behavior displays features associated with both extremes. This hybrid or "leathery" response is observed in polymeric systems near their glass-transition temperature. The processes associated with deformation in this regime are complex in that both thermal activation and structural relaxation must be considered in any theory attempting to explain the behavior.

The present simulations incorporate 50−100 Monte Carlo cycles between 0.0025 strain increments, giving a total of O(1e5) minimization cycles attempted during deformation up to 70% true strain. (A typical deformation simulation of a 12 000 particle system took approximately 12 CPU hours on a DEC Alpha 267 MHz machine. The preparation of the initial structure typically requires 24−40 CPU hours on the same system.) There is no direct way to actually correlate these cycles with a real time scale. Comparisons between these simulations and typical (MD) simulations (e.g., see Brown and Clarke[15]) in which a similar number of time steps are used to obtain similar levels of strain suggest that the deformations mimicked by the Monte Carlo procedure physically represent strain rates on the order of 10^8-10^9 s^{-1}. The stress−strain responses clearly indicate that a deformation state which induces high pressures (i.e., plane strain compression) produces a high-equivalent shear flow stress whereas a deformation state which induces low or negative pressures (i.e., uniaxial tension) produces a relatively low equivalent flow stress. These results are consistent with what would be observed in a polymer in either the glassy or leathery regime. Physically, the sensitivity in glassy/leathery polymers reflects the effects of applied pressure on structural energy barriers. In the isostructural limit (i.e., very low temperatures or very high strain rates), applied pressure enhances the barriers to the relatively, accessible bond torsion motions by making dilation of the local atomic environment more difficult, as discussed by Mott et al.[11] Thus larger applied shear stresses are required before generation of flow is possible.

The state of deformation sensitivity observed from the simulations shown coupled with the high representative strain rates suggest that the behavior reproduced by the model at $T^* = 0.2841$ captures basic features characteristic of isostructural or glassy deformation. Although a temperature of $T^* = 0.2841$ indicates that the available thermal energy is on the same order as the energy well for a single Lennard-Jones pair interaction (roughly a 1−4 ratio of thermal energy to well depth), the strain rates probed by the simulations appear to be too high for significant structural relaxation to occur between strain increments.

A direct assessment of the characteristic times (or more precisely the number of Monte Carlo cycles) associated with structural relaxation phenomena in the model can in principle be obtained by simulation of dynamic mechanical experiments. Unfortunately, present computational resources are insufficient to carry out such a formidable task which requires repeated cycling of loading conditions over a wide range of temperatures and "frequencies". Instead, internal energy changes observed during deformation are used as an indicator of the type of behavior being reproduced by the model. The increases in internal energy with strain shown in Figure 9 clearly suggest that structural relaxation is not occurring rapidly enough to offset the energy build up due to deformation-induced distortion of the bonded/nonbonded degrees of freedom. This is evident from the energy changes observed upon unloading, which show the bond angle bending, bond torsion, and intermolecular energy values remaining at higher than predeformation levels. Although it is likely that entropic effects play some role in determining the response of the model under the simulated conditions, the locking in of torsion angle and bond angle distortions as well as intermolecular spacing changes shows that structural relaxation on the time scale of the applied deformation is not dominating the model behavior. This notion of deformation-induced internal energy storage is consistent with observations from differential scanning calorimetry experiments (DSC) on typical glassy polymers such as polycarbonate, poly(methyl methacrylate) (PMMA), and polystyrene specimens deformed to various levels of strain.[36]

In the context of the discussion above, the responses obtained by varying the number of minimization cycles between strain increments at $T^* = 0.2841$ shown in Figure 9 thus represent strain rate effects on mechanical behavior which fit in the framework of stress-biased, thermally activated processes. As argued above, the applied strain rates are high enough that the behavior falls near the isostructural limit. The rate effect comes about because of the imposed limitation on the amount of time the system is allowed to sample a particular structural state. Controlling the number of Monte Carlo cycles (i.e., "time") that the system is allowed to sample

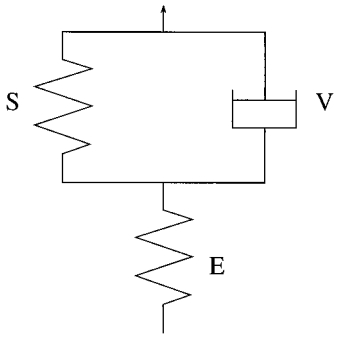

Figure 15. Schematic representation of network elements used to model glassy polymers in a continuum framework in Haward and Thackray. E denotes the linear elastic element; V denotes the viscous element; and S denotes the network orientation element.

also effectively controls the number of material "sites" at each state (a quantity estimated through the use of transition-state theory), thus allowing the system to mimic rate effects during deformation.

The behavior described above is in strong contrast to the results obtained from deformation simulations at $T^* = 2.841$ at similar strain rates. Although the macroscopic stress−strain response of the network at $T^* = 2.841$ shares some features with the response obtained at $T^* = 0.2841$ (strain softening, extended flow region), the internal energy changes at this temperature suggest that there are fundamental differences between the two cases. The relatively low flow stress values and the apparent constancy of internal energy quantities indicate that the behavior is phenomenologically attributable to a viscous type dissipation mechanism or configurational entropy effects or both. Structural relaxation is presumably occurring so rapidly that the system is able to reach thermodynamic equilibrium during deformation. In the context of the example discussed previously, thermal fluctuations are occurring rapidly enough that any deformation-induced free energy barrier biases have little effect on the equilibrium distribution of state populations.

6.2. Stress Partitioning Evolution. The previous discussions regarding overall mechanical response of the polybead model network still leave open the question of how the different types of interactions (intra- and intermolecular) and their relative contributions to the macroscopic behavior evolve with deformation. Although investigations such as those by Boyce et al.[5,37] attempt to address this issue in a continuum constitutive modeling context, relatively few efforts have been made to explicitly determine the exact manner in which the relative contributions develop. Boyce argues that the behavior of a glassy polymer can be considered to be a result of a combination of inter- and intramolecular forces which can be schematically represented as a large deformation theological network of the type first proposed by Haward and Thackray[38] (Figure 15). At small strains, the elastic response is assumed to be a result of intermolecular interactions which are represented by the elastic element labeled E. During yield and steady state flow, Boyce suggests that the observed strain softening and flow is due primarily to an evolution of material structure which acts to reduce the magnitude of intermolecular barriers (represented by element V) to segmental rotation until reaching a steady-state condition. As the intermolecular barrier to flow is overcome and proceeds to soften, the rotation of the chain segments leads to the parallel development of orientation-induced strain hardening (element S).

The results shown in Figures 11 and 12 are believed to be the first calculations illustrating the relative contributions of various interactions to the macroscopic response in a dense amorphous polymer system. Although the analysis of Mott et al.[11] showed the level of internal stresses to be extremely high, their work does not provide an explicit breakdown of the various contributors to stress. As discussed previously, the initial average intermolecular stress is highly compressive whereas the initial average intramolecular stress is highly tensile. Calculations during the deformation simulations have shown that the signs of each contribution do not change. For clarity, the contributions from intermolecular forces, intramolecular forces, and thermal motion to the total stress response are shifted in the figures so that each component begins at the origin. The results show an initially stiff elastic response dominated by both inter- and intramolecular contributions followed by the onset of flow characterized by a leveling off and then softening of the intermolecular contribution while the intramolecular contribution continues to increase. These results strongly support the continuum-level approach used by Boyce et al.[5,37] The softening behavior exhibited by the intermolecular stress component is a result of several possible factors. Changes in mean particle spacing in the direction of loading can influence the intermolecular stress in that direction. Reduced spacing elevates intermolecular compression whereas increased spacing relieves it. For the data shown in Figure 11, this suggests that mean particle spacing is decreasing in the direction of loading during the strain softening regime of the response. Given that the density is approximately constant during flow, it is unlikely that this is occurring. Another possibility may be that the distribution of local densities may be changing in such a way that softening occurs while the average particle spacing remains unchanged. Although the analysis of Mott et al.[11] of pressure changes during deformation indicates that temporary dilation occurs during passage of a glassy structure over a saddle point configuration, their results do not suggest that evolution of the local free volume distribution directly causes the strain softening phenomena. Recalling Figure 12, the stress partitioning obtained during deformation of the network at $T^* = 0.2841$ under uniaxial tension conditions was found to be qualitatively similar to compressive behavior in that the intramolecular stress increases monotonically, and the strain softening effect is a result of intermolecular stress softening. The nearly constant volume nature of this deformation also indicates that if softening is a volume effect, it must be due to some redistribution of local densities. Attempts to find such a redistribution by constructing contour plots of local densities were unsuccessful, even though contour plots of local strains were revealing.[39]

A more likely and physically plausible explanation for the softening is the occurrence of structural instabilities that are continually relieved through the application of shear deformation. Following arguments analogous to those presented by Mott,[12] the phenomena is more clearly visualized if intermolecular softening is considered to occur in a series of discrete steps. Figure 16 had depicted a representative response of both inter- and intramolecular contributions to the mechanical behavior

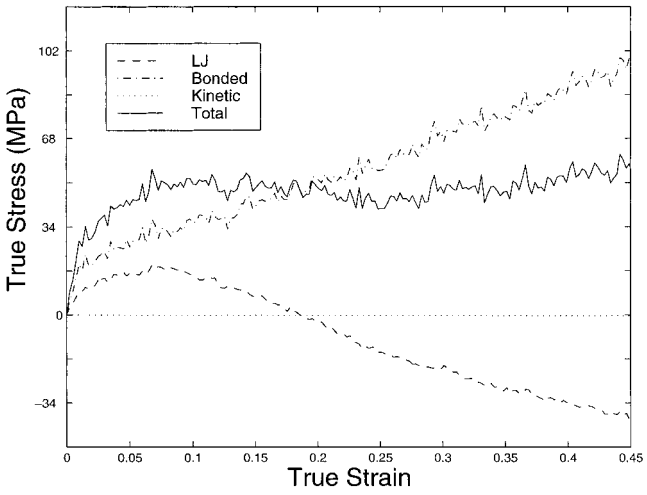

Figure 16. Partitioning of stress for network at $T^* = 0.284$ under uniaxial tension conditions with data shifted for clarity.

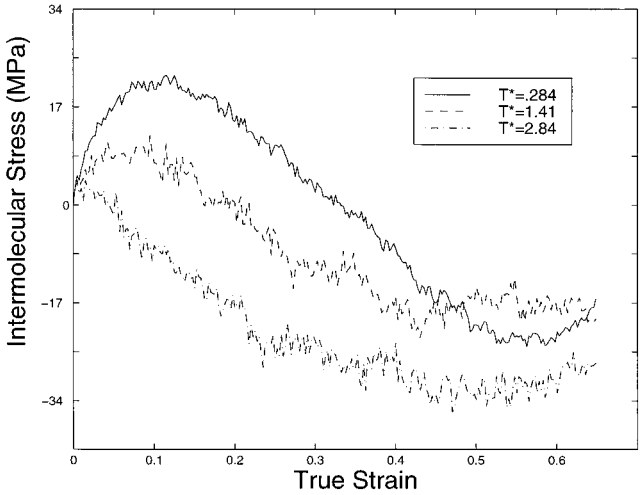

Figure 17. Evolution of intermolecular stress at three temperatures.

in the glassy state. Both contributions increase with applied deformation in a stable fashion until reaching the peak in the overall stress−strain curve. At the initial peak, the structure becomes unstable and jumps to a configuration corresponding to a local free energy minima, creating a drop in the intermolecular stress in the process. The process proceeds as a continual sequence of deformation driven jumps over local free energy barriers to lower free energy configurations, thus producing the intermolecular strain softening effect. After the system is driven to a sufficiently low free energy state, subsequent jumps from minima to minima no longer reduce the overall free energy of the structure. At this point, the structure produces steady-state intermolecular flow behavior, as shown by the relatively constant intermolecular stress. The simulations indicate that the total drop in intermolecular stress between the initial peak and the steady-state value can be larger than the intermolecular stress increase obtained in reaching the first peak! The monotonically increasing intramolecular stress appears to provide stability during the process by providing the structure with additional resistance to deformation. A detailed description of how various structural features evolve with deformation is provided in related publications (see Chui[40] and Chui and Boyce[41]).

The sensitivity of the observed intermolecular stress softening to changes in temperature is shown in Figure 17, which plots the changes in intermolecular stress with temperature for simulations at three temperatures. The lowest temperature response corresponds to the isostructure case discussed in the previous two paragraphs for which the highest temperature response corresponds to the viscous or "rubbery" behavior($T^* = 2.841$). Results from a simulation at an intermediate temperature($T^* = 1.42$) are also shown. The data indicates that temperature has a significant effect on the magnitude of the drop in intermolecular stress during strain softening with smaller drop occurring at $T^* = 1.42$ than that observed at $T^* = 0.2841$. Physically, this can be interpreted as meaning that the structure begins closer to an equilibrium state at higher temperatures, thus reducing the amount of free energy falling required before reaching a stable steady-state flow condition. Structural relaxation is probably simultaneously occurring, enabling the system to more readily achieve an equilibrium state. At this temperature, the system still exhibits some features of isostructural behavior in that the intermolecular response initially increases with strain until reaching a peak, after which softening effects develop. At the highest temperature ($T^* = 2.841$), no such increase is observed. The intermolecular stress exhibits softening immediately, indicating that the initially metastable structure requires little mechanical assistance before marching towards a more stable state. That there is any evolution at all in the intermolecular stress at this temperature suggests that the system is not truly probing rubbery or thermodynamic equilibrium behavior but is instead still reproducing a response characteristic of the transition regime (i.e., leathery) behavior. Simulations at much higher temperatures ($T^* > 10.0$) appear to be necessary before true rubbery behavior can be obtained.

7.0. Summary of Results and Conclusions

7.1. Model Development. A polybead network model of amorphous polymers has been developed. The chain interaction parameters are set so that bond stretching and bond angle bending are much stiffer than bond torsion. Long-range interactions and steric hindrance are introduced by incorporating intermolecular interactions of the Lennard-Jones-type which mimic short-range repulsion and long-range attraction and act to bias conformers towards the trans state.[43]

By using a variation of previously developed random walk-based chain growth techniques,[9] structures with fairly low bonded energies can be initially generated. The network generation algorithm is sufficiently general so that networks with a wide range of topological properties can be modeled through proper specification of parameters such as cross-link functionality, cross-link junction density, molecular weight distribution, and cross-link tolerance distance.

The networks are evolved through use of the Metropolis algorithm[28] under isothermal−isochoric and isothermal−isostress conditions. By using closed-loop feedback control, mixed displacement and traction boundary conditions are maintained efficiently. Deformation is imposed on the networks through affine strain increments followed by some number of Monte Carlo cycles, thus producing rather heterogeneous overall particle motions. By controlling the number of Monte Carlo cycles allowed between strain increments, the effects of deformation rate are mimicked.

Equilibration of the initial structures is quite involved, with a series of steps involving annealing, cooling, and mechanical conditioning required to produce suitable systems. As shown in subsequent deformation simulations, the preparation schedule appears to be effective in creating networks which produce mechanical behavior representative of amorphous polymers.

7.2. Initial Structure. The networks display spatial correlations in structure appropriate for glassy materials with strong short-range correlations representative of inter- and intrachain first- and second-neighbors and weak long-range correlations representative of random motion. Comparisons between bonded distributions of single-chain and network systems indicate that the long-chain structures contain a small fraction of bond angles which are flexed to a greater extent than is attributable to thermal motion, indicating that the constraints of the long-chain system hinder relaxation of the system.

Stresses in the network are a result of thermal motion, bonded forces, and nonbonded (i.e., intermolecular) forces. Calculations for single-chain and network systems under pressure-free conditions at various temperatures show that bonded contributions are always tensile and nonbonded contributions are always compressive (i.e., repulsive), suggesting that the locking in of tensile bonded forces and compressive intermolecular forces is a general feature of densely entangled chain systems.

7.3. Macroscopic Mechanical Response. The macroscopic mechanical response of the polybead model qualitatively captures the proper state of deformation, rate of deformation, and temperature dependencies found for real amorphous polymeric materials. Specifically, states of deformation which generate relatively high hydrostatic pressures such as plane strain compression and uniaxial compression produce higher flow stress values than do other states of deformation, such as uniaxial tension, which are subject to negative hydrostatic pressures. Increasing temperature lowers flow stress through the enhancement of structural relaxation. Increasing the rate of deformation increases the flow stress by reducing the amount of time allowed for the system to relax between strain increments. The behavior can be generalized by stating that conditions which reduce the mobility of the chains (i.e., decreasing temperature, or increasing pressure) relative to the rate of deformation tend to elevate the resulting macroscopic flow stress. The rates of deformation mimicked by the simulations are believed to be high enough that the model samples glassy (isostructural) and leathery (transition) behavior at the lowest and highest investigated temperatures, respectively. The regimes of behavior probed manifest themselves in internal energy measures which show significant increases during deformation of the glassy system and much smaller increases during deformation for the leathery system.

The investigation of the evolution of the various contributors to stress (i.e., intermolecular, intramolecular, thermal motion) during deformation found that the strain softening observed in the overall response is attributable solely to drops in the intermolecular contribution to stress. The decrease is believed to be a result of the system evolving from an initially high free energy metastable state to lower free energy state during deformation. The magnitude of the drop depends on the temperature, in that systems prepared at very low temperatures are likely to begin at a relatively high free energy local minimum, which means that larger free energy drops and hence larger intermolecular stress drops are required to reach a stable structural state. The intermolecular barrier is observed to be somewhat lower in uniaxial tension then in uniaxial compression, thus explaining the origin of the pressure dependence of yield. The evolution of the intramolecular contribution to stress is found to be stronger in uniaxial tension than uniaxial compression, thus explaining/confirming the state of deformation dependence of postyield strain hardening. These results provide a molecular basis for the assumptions used in continuum-level constitutive modeling of Boyce et al.[37] and Arruda and Boyce[5] and explain the success of these models in capturing finite strain deformation of amorphous polymers.

The MC modeling technique presented in this paper has been found to successfully capture the significant structural features of amorphous polymers, as well as the deformation behavior over a wide range of loading conditions. The evolution in specific chain kinematics corresponding to the studied deformation are discussed in related work (Chui[40] and Chui and Boyce[41]). The success of this approach motivates future studies in which, for example, specific structural features could be varied and their impact on macroscopic mechanical behavior could be directly assessed.

Acknowledgment. This research has been funded by the U.S. National Science Foundation through Grants DMM9157899 and MSS9215805. C.C. also gratefully acknowledges a fellowship from the Kodak Foundation.

References and Notes

(1) Bunn, C. In *Molecular Behavior and the Development of Polymeric Materials;* Ledwith, A., North, A., Eds.; Chapman and Hall, Ltd: New York, 1974.
(2) Arridge, R. *Mechanics of Polymers*; Clarendon Press: Oxford, 1975.
(3) Crist, B. In *The Physics of Glassy Polymers*; Haward, R. N., Young, R. J., Eds.; Chapman and Hall: London, 1997.
(4) Boyce, M. C.; Haward, R. N. In *The Physics of Glassy Polymers*; Haward, R. N., Young, R. J., Eds.; Chapman and Hall, London, 1997.
(5) Arruda, E. M.; Boyce, M. C. *Int. J. Plast.* **1993**, 9, 697.
(6) Deng, D.; Argon, A. S.; Yip, S. *Philos. Trans. R. Soc. London* **1989**, *A329*, 613.
(7) Maeda, K.; Takeuchi, *S. Philos. Mag.* **1981**, *A44*, 643.
(8) Srolovitz, D.; Vitek, V.; Egami, T. *Acta Metall. Mater.* **1983**, *31*, 335.
(9) Theodorou, D.; Suter, U. *Macromolecules* **1985**, *18*, 1467.
(10) Theodorou, D.; Suter, U. *Macromolecules* **1986**, *19*, 139.
(11) Mott, P.; Argon, A. S.; Suter, U. *Philos. Mag.* **1993**, 67, 931.
(12) Mott, P. Atomistic Modeling of Deformation of Glassy, Atactic Polypropylene. Ph.D. Thesis, Massachusetts Institute of Technology, Cambridge, MA, 1992.
(13) Hutnik, M.; Argon, A. S.; Suter, U. *Macromolecules* **1993**, *26*, 1097.
(14) Hutnik, M. Simulation of the Structure and Inelastic Behavior of Dense, Amorphous Bisphenol-A Polycarbonate. Ph.D. Thesis, Massachusetts Institute of Technology, Cambridge, MA, 1991.
(15) Brown, D.; Clarke, **J.** *Macromolecules* **1991**, *24*, 2075.
(16) McKechnie, J.; Clarke, J. *Macromolecules* **1993**, *26*, 198.
(17) Binder, K.; Heermann, D. *Monte Carlo Simulation in Statistical Physics: An Introduction*; Springer-Verlag: 1992.
(18) Curro, *J. J. Chem. Phys.* **1971**, *61* (3), 1204.
(19) Gao, J.; Weiner, J. *Macromolecules* **1987**, *20*, 2520.
(20) Gao, J.; Weiner, J. *Macromolecules* **1987**, *20*, 2525.
(21) Rigby, M.; Smith, E.; Wakeham, W.; Maitland, G. *The Forces Between Molecules*; Clarendon Press: Oxford, 1986.
(22) Sylvester, M. Molecular Dynamics Studies of the Liquid−Glass Transition in Atactic Poly(propylene). Ph.D. Thesis,

Massachusetts Institute of Technology, Cambridge, MA, 1992.
(23) Ogura., I.; Yamamoto, T. *Polymer* **1995**, *36*, 1375.
(24) McKechnie, J.; Brown, D.; Clarke, J. *Macromolecules* **1992**, *25*, 1562.
(25) Grest, G.; Kremer, K.; Duering, E. *Europhys. Lett.* **1992**, *19*, 195.
(26) Duering, E.; Kremer, K.; Grest, G. *Macromolecules* **1993**, *26*, 3241.
(27) Lobe, B.; Baschnagel, J.; Binder, K. *J. Non-Crystal. Solids* **1994**, *172-174*, 384-390.
(28) Metropolis, N.; Rosenbluth, A.; Rosenbluth, M.; Tellar, A.; Teller, M. *J. Chem. Phys.* **1953**, *21*, 1087.
(29) Heerman, D. W. *Computer Simulation Methods in Theoretical Physics*; Springer-Verlag: Berlin, 1986.
(30) Wignall, C. D.; Longman, G. W. In *Physical Structure of the Amorphous State*; Allen, G., Petrie, S.E.B., Eds.; Marcel Dekker, Inc.: New York, 1977.
(31) Boyce, M. C.; Arruda, E. M.; Jayachandran, R. *Polym. Eng. Sci.* **1994**, *34*, 716.
(32) Gao, J.; Weiner, J. *Macromolecules* **1991**, 24, 1519.
(33) Spaepen, F.; Turnbull, D. In *Metallic Glasses*; American Society for Metals: Metals Park, OH, 1978.
(34) Argon, A. S. *Philos. Mag.* **1973**, *28*, 8.
(35) Doi, M.; Edwards, S. *The Theory of Polymer Dynamics*; Clarendon Press: Oxford, 1986.
(36) Hasan, O. A.; Boyce, M. C. *Polymer* **1993**, 34, 5085.
(37) Boyce, M.; Parks, D. M.; Argon, A. S. *Mech. Mater.* **1988**, 7, 15.
(38) Haward, R.; Thackray, G. *Proc. Royal. Soc. London* **1968**, *302*, 453.
(39) Chui, C.; Boyce, M.C. *J. Non-Crystal. Solids* **1998**, *235−237*, 612.
(40) Chui, C. Application of Monte Carlo Techniques to the Study of Amorphous Polymer Deformation. Ph.D. Thesis, Massachusetts Institute of Technology, Cambridge, MA, 1998.
(41) Chui, C.; Boyce, M. C. *Monte Carlo Modeling of Amorphous Polymer Deformation: Evolution of Structure with Strain* 1999, in preparation.

MA9815399